LIGO-P070152-P

Diagonalization of the length sensing matrix of a dual recycled laser interferometer gravitational wave antenna

Shuichi Sato* and Seiji Kawamura
TAMA project, National Astronomical Observatory of Japan, 2-21-1, Mitaka, Osawa, Tokyo 181-8588 Japan

Keiko Kokeyama and Fumiko Kawazoe
The Graduate School of Humanities and Sciences, Ochanomizu University, 2-1-1, Otsuka, Bunkyo-ku, Tokyo 112-8610 Japan

Kentaro Somiya
Max-Planck-Institut für Gravitationsphysik, Am Mühlenberg 1, 14476 Potsdam, Germany
(Received 18 October 2006; published 26 April 2007)

Next generation gravitational wave antennas employ resonant sideband extraction (RSE) interferometers with Fabry-Perot cavities in the arms as an optical configuration. In order to realize stable, robust control of the detector system, it is a key issue to extract appropriate control signals for longitudinal degrees of freedom of the complex coupled-cavity system. In this paper, a novel length sensing and control scheme is proposed for the tuned RSE interferometer that is both simple and efficient. The sensing matrix can be well diagonalized, owing to a simple allocation of two rf modulations and to a macroscopic displacement of the cavity mirrors, which cause a detuning of the rf modulation sidebands.

DOI: 10.1103/PhysRevD.75.082004 PACS numbers: 04.80.Nn, 42.60.Da, 95.55.Ym

I. INTRODUCTION

Currently existing terrestrial interferometer gravitational wave (gw) antennas [1], which are categorized as first generation detectors, are currently going on-line for searching gravitational waves. First detection and direct observation of gravitational waves are primary goals and would be a landmark achievement in physics. However, the next ambition is opening a window to gravitational wave astronomy, a brand-new field of view to the universe. Differing from an electromagnetic wave, the gw has only faint interaction with matter, so extremely high sensitivities, reaching, or overcoming the standard quantum limit (SQL) are required for the next generation detectors. Planned detectors such as Advanced-LIGO (AdLIGO) [2] or the Japanese LCGT [3] can be considered second generation gw detectors, whose sensitivity is reaching to or will slightly surpass the SQL, by using various techniques; for example, an advanced optical configuration, advanced mirror materials, a different beam profile, and cryogenics.

AdLIGO and LCGT will employ an optical configuration called "resonant sideband extraction" (RSE) [4], which is realized with an additional signal-extraction mirror (SEM) added to the power-recycled Fabry-Perot Michelson interferometer (FPMI). It is placed between the beam splitter and the dark port, as shown in Fig. 1. The laser light resonates inside the two arm cavities and the power-recycling cavity, in a way identical to first generation gw detectors employing power-recycled FPMI. If the laser light is antiresonant inside the signal-recycling cavity (without arm cavities), this is called "signal recycling," which is one of the operation modes of the dual-recycled FPMI. In contrast, if the carrier is resonant inside the signal-recycling cavity, as in the case of LCGT, this mode is called resonant sideband extraction (tuned RSE), and if the carrier is kept slightly off-resonant from tuned RSE (or signal-recycled FPMI) by microscopic displacement of the signal-recycling mirror position, it is called detuned RSE (or "detuned signal-recycling") as in the case of AdLIGO.

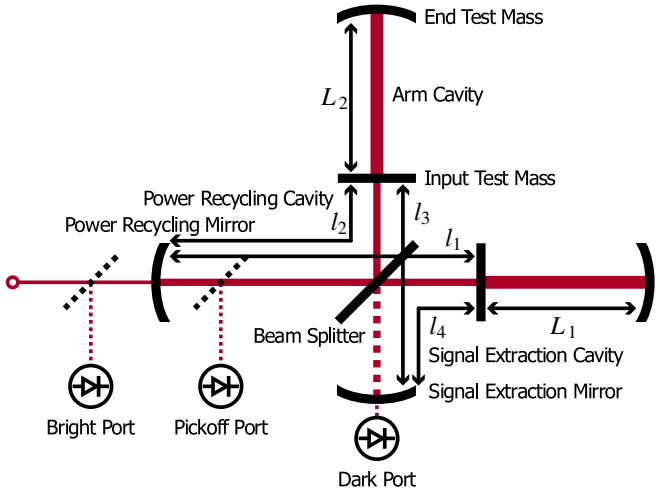

FIG. 1 (color online). The schematic of the RSE interferometer optical configuration. The power-recycling mirror (PRM) is placed between the beam splitter and the laser source to enhance the circulating laser power inside the interferometer, whereas the signal-extraction mirror (SEM) is placed between the beam splitter and the dark port to enhance the detector response, which makes the whole interferometer system more complex. The length degrees of freedom and the control signal-extraction ports are shown in addition to the optical arrangement.

*Electronic address: sato.shuichi@nao.ac.jp

The most significant reason for adopting the RSE configuration for LCGT is a thermal problem. LCGT plans to use cryogenic test masses around 20 K, and so the heat dissipation due to losses of the laser power in the mirror substrates can become a serious problem. By increasing the finesse of the arm cavities and by implementing RSE, one can reduce the circulating power in the power-recycling cavity while maintaining shotnoise-limited sensitivity. One of the merits of RSE for AdLIGO is also a thermal issue. RSE can reduce the heat dissipation inside the mirror substrates and accordingly suppress the thermal lensing effect that can cause an imperfect interference at the signal detection ports. Another merit for AdLIGO is that the shotnoise level at the particular frequency band of interest can be improved by using detuned RSE [2]. This is a very significant feature for particular gw sources such as mergers of compact binary systems.

Only when all of the test masses and other interferometer optics are kept at appropriate positions to make the laser light resonant and interfere properly inside the interferometer, the interferometer works as a gw antenna, producing a linear signal proportional to the gw strain. Therefore, precise position control of the optics is indispensable for keeping the interferometer operational. Thus, one of the most important roles of the signal sensing scheme is to provide appropriate error signals for the degrees of freedom to be controlled. When the system is multi-degree-of-freedom and needs multiloop control, the mixing of signals with each other could cause serious problems [5]. The primary goal of this study is, therefore, to extract a diagonal sensing matrix, providing appropriate error signals independently without a signal admixture of other degrees of freedom.

In this paper, the emphasis is placed on the description of a sensing scheme that gives a diagonal sensing matrix, and an optimization of the optical configuration parameters of RSE using both analytical and numerical simulations. The numerical simulations were performed using FINESSE simulation software [6]. This scheme was originally developed on the assumption of implementation for tuned RSE; however, it could also be applicable for detuned RSE.

II. REVIEW OF THE LENGTH SENSING AND CONTROL SCHEME

The baseline of the signal sensing method for the RSE interferometer is to use the Pound-Drever-Hall (PDH) [7] technique and its extended scheme; using different wavelengths of light which behave differently for each optical system. Therefore, the main issue of designing a signal sensing scheme is to determine the modulation and demodulation scheme, the arrangement of modulation sidebands. In this sense, the sensing scheme is associated one to one with the arrangement of the rf modulation(s); the number of the modulations, the resonance conditions of the modulations inside cavities, and the Schnupp asymmetry factor [8].

For the first generation interferometers, an extended PDH technique is commonly used as the signal sensing method. The laser light is phase modulated at an rf frequency before illuminating the interferometer, then the light from the appropriate signal-extraction ports is photodetected and demodulated with a rf local signal to extract the sensing signals. Efficient signal extraction is achieved with intentional macroscopic asymmetry for the Michelson interferometer arm lengths, which is called premodulation or Schnupp modulation technique for a gw interferometer application. The total number of longitudinal degrees of freedom to be controlled for the power-recycled Fabry-Perot Michelson interferometer configuration is four: common and differential length of the arm cavities, power-recycling cavity (PRC) length, and Michelson differential length. In order to extract the four sensing signals, a single rf phase modulation and three signal-extraction ports (bright, dark and pickoff ports) are dedicated.

On the other hand, for the RSE configuration, with the additional signal-recycling mirror, there are five longitudinal degrees of freedom to be controlled, which are defined in Table I. The addition of the extra mirror makes the interferometer a more complex, multiply coupled-cavity system, which consists of arm cavities, power- and signal-recycling (extraction) cavities.

In connection with the additional degrees of freedom, a double modulation and demodulation scheme (DMD) was introduced to the gw laser interferometer. By introducing another set of modulation sidebands, there are increased combinations of beat signals between carrier and modulation sidebands. The conventional single modulation scheme extracts the signals from the beating between the carrier and the phase modulation sidebands, whereas DMD utilizes the beating between two modulation sidebands at different frequencies (see Appendix A).

In preparation of an eventual realization of the advanced optical configuration, there were several tabletop experiments of RSE systems to study the sensing and control method, and to demonstrate the feasibility of the dual recycling with FP cavities: Caltech [9], Florida [10], and Australia [11]. These are all for a detuned operation of

TABLE I. The definition of length degrees of freedom, which are defined as modulo wavelength of the laser λ, whereas Schnupp asymmetry is defined as macroscopic length.

Name	Symbol	Definition	Derivative
Common arm length	L_+	$L_1 + L_2$	δL_+
Differential arm length	L_-	$L_1 - L_2$	δL_-
PRC length	l_p	$l_1 + l_2$	δl_p
Michelson length	l_-	$l_1 - l_2$	δl_-
SEC length	l_s	$l_3 + l_4$	δl_s
Schnupp asymmetry	l_{sch}	$l_1 - l_2$	

RSE, i.e. AdLIGO, and a prototype experiment on the 40 m interferometer at Caltech [12], and the 4 m interferometer at the National Astronomical Observatory of Japan are now in progress [13].

For the most appropriate design of the signal sensing system, many factors should be carefully considered:

(i) Diagonal sensing matrix: It is ideal that five error signals for longitudinal degrees of freedom are extracted independently, without significant cross talk with other signals.

(ii) Robust signal extraction: The signal sensing matrix should be robust enough to any possible imperfections and asymmetry of the interferometer.

(iii) Less noise coupling: Some of the noises appear at the signal readout port in combination with the parameters that the sensing design had intended, and therefore the noise coupling efficiency should be suppressed low enough.

(iv) Easy lock acquisition: The whole interferometer system should be rendered operational easily from an uncontrolled state. The dynamical nature of the five error signals are important during the lock acquisition process.

Suppose there is a system with i degrees of freedom that are to be controlled, and there is an identical number i of extracted signals. In general, each of these signals can have some sensitivity for all i degrees of freedom. However, they should be linearly independent from each other at least in principle, so that they could close stable feedback loops. Furthermore, it is well known that the feedback signals should be as diagonal as possible to ensure a robust control of the system.

There are two ways of diagonalization: optically diagonal state and electronically diagonal state. If each of the extracted signals is sensitive to only one of the degrees of freedom, this case is called an optically diagonal state. Whereas, if the extracted signals are linearly independent, it is possible to reconstruct a diagonal state by manipulating the signals electronically (or digitally on the computer), which is referred to as an electronically diagonal state.

As far as control signals are concerned, both are thought to be almost equivalent; however, the optically diagonal state might have some potential advantages when the signal to noise ratio, dynamical nature of lock acquisition, and robust control of the systems are taken into account. Therefore, among these points of view, the emphasis was especially placed on the optically diagonal sensing of the five error signals for the longitudinal degrees of freedom, because that is where the true advantage of this signal sensing lies. In the following sections, the above items are discussed in connection with the newly proposed signal sensing scheme.

Summarizing the argument, RSE needs an appropriate signal sensing and control scheme for five longitudinal degrees of freedom, which should be good enough for such requirements as a diagonal sensing matrix, robust signal extraction, less noise coupling, and easy lock acquisition. The thing to be considered first is a signal separation (diagonal sensing matrix in its ultimate sense) in a sense that the control scheme should work properly. Both electronic diagonalization using nondiagonal sensing signals and optical diagonalization should work well in principle; however, the authors think that the optically diagonal state might have some potential advantages. To confirm that, a prototype experiment for demonstration of tuned RSE is under way at the National Astronomical Observatory of Japan [13].

III. DIAGONALIZED SIGNAL SENSING

A. Allocation of modulations

L_+ and L_-, the common and differential arm cavity length signals, are expected from the premodulation signal sensing scheme, beating the carrier and phase modulated sideband fields. The significant enhancement of the carrier field inside the two arm cavities results in huge phase sensitivities in extracting the signals for L_+ and L_-. This means both L-signals can be extracted relatively independently, without much admixture of any other longitudinal signals, or in other words, the sensing matrix for them is almost diagonal. On the other hand, for the l_p, l_s, and l_- signals of the central part of the RSE interferometer, it is known from preceding studies that extracting independent signals is not easy. Therefore, the main issue here is to identify a sensing scheme that enables a diagonal sensing matrix.

By analyzing the optical configuration of RSE closely, the complicated optical system turns out to be an intricately connected cavity system. Furthermore, when one concentrates on the central part of the interferometer, consisting of input test mass, recycling mirrors, and beam splitter, the dual-recycled Michelson interferometer can be regarded as a coupled cavity (Fig. 2). Thus the issue is now reduced to the signal extraction of the coupled cavity.

One of the important features of the PDH scheme is to make use of different responses (or, equivalently, different field enhancements) of the optical fields inside optical systems. Therefore, a different arrangement of the two sets of sidebands for the coupled cavity is essential. The simplest, straightforward, and natural allocation would be that one of the sidebands circulates both inside PRC and signal extraction cavity (SEC) , whereas the other sideband resonates only inside the PRC, as is shown in Fig. 2. The l_s signal could be extracted due to the above difference between the two sidebands; in contrast, the l_p signal could be obtained making use of the difference of field enhancements inside the PRC.

The concepts of the suggested signal-extraction scheme can be summarized in the following:

LIGO-P070152-P
PHYSICAL REVIEW D 75, 082004 (2007)

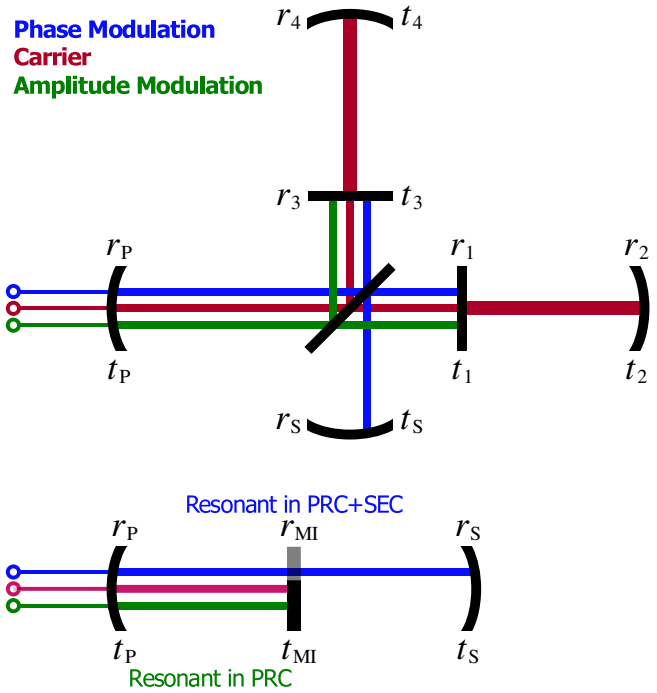

FIG. 2 (color online). Resonant conditions for optical fields, carrier, and modulation sidebands. Optical fields are color coded. The legend in the upper left indicates the order of the fields, entering the interferometer from the left (laser). The carrier field resonates inside both arm cavities and the power-recycling cavity, which gives enhanced response to gravitational wave signals. The phase modulation is designed to circulate inside the power-recycling and the signal-extraction cavity, whereas the amplitude modulation circulates only inside the power-recycling cavity. The central part of RSE, the dual-recycled Michelson interferometer, can be viewed as a coupled cavity, as is shown in the lower figure. The coupling connecting the two cavities is indicated by a plane mirror representing the Michelson interferometer.

(i) PM (phase modulation) sidebands are completely transmitted by the Michelson interferometer (MI) and resonate inside the PRC + SEC.
(ii) AM (amplitude modulation) sidebands are completely reflected by the MI, and resonate only inside the PRC.

The PM should circulate inside both PRC and SEC to reach to the dark port so that it can be used as a local field against the carrier field for the L_- signal extraction using a conventional PDH technique; whereas the AM can be a local field against the PM field on double demodulation scheme. The second modulation must be AM in case of tuned RSE so that the beating between two modulations can produce error signals. However, it can be PM again in the case of detuned RSE, because the detuning of the carrier inside the SEC can make the phase modulation sidebands have unbalanced resonances, which would produce separate beat signals. The point of this modulation scheme is that the arrangement of the modulation sidebands is very simple, using complete transmission and reflection at the Michelson interferometer, which enables clean signal extractions especially for the l-signals.

In order to realize the sidebands allocation as shown in Fig. 2, the optical property of the coupling mirror (Michelson interferometer for the case of RSE) of the coupled-cavity system could be a key factor. The major difference between a simple coupled cavity and the central part of RSE is that the coupling mirror can be made to have variable reflectivities. The reflectivity and the transmissivity of the Michelson interferometer for the RSE for modulation sidebands are functions of the jth modulation frequency ω_j and the Schnupp asymmetry $l_{\rm sch}$, and they are defined as $r_{{\rm MI}j} = \cos\alpha_j$ and $t_{{\rm MI}j} = {\rm i}\sin\alpha_j$ with an asymmetry factor $\alpha_j = l_{\rm sch}\omega_j/{\rm c}$. Therefore, in general, two sets of sideband fields with different modulation frequencies may have different reflectivities and transmissivities for the Michelson interferometer. For PM and AM, satisfying the above conditions, the following constraints are imposed:

(i) PM: $r_{\rm MI1} = 0$ with $l_{\rm sch}\omega_{\rm m1}/{\rm c} = \pi/2 + n\pi$,
(ii) AM: $r_{\rm MI2} = 1$ with $l_{\rm sch}\omega_{\rm m2}/{\rm c} = n'\pi$,

where n and n' are integers. The control signal-extraction ports are assumed to be at bright, pickoff, and dark port (transmitted light from SEM), which is the same as for first generation gw antennas. Using a double-modulation and -demodulation procedure, as described in Appendix A, the analytic expressions for signal sensitivities on longitudinal degrees of freedoms are given as follows. To simplify the full expressions, several optical and other parameters were defined in a conventional way:

(i) r_x and t_x: amplitude reflectivity and transmissivity of the optics x. The $x = {\rm p}, {\rm s}$ denotes power recycling and signal-extraction mirror, respectively.
(ii) r_{xy}: amplitude reflectivity of an optical system, for field y at port x. The $x = {\rm a}, {\rm p}$ denotes arm and power-recycling cavity, whereas $y = 0, 1, 1{\rm u}, 1{\rm l}, 2, 2{\rm u}, 2{\rm l}$ denotes carrier, first modulation sideband, upper and lower sideband of those, second modulation sideband, upper and lower sidebands of those, respectively. The reflectivity of the arm cavities for the PM sidebands (sideband 1), for example, is given as $r_{\rm a1} = (-r_1 - r_2)/(1 + r_1 r_2)$, where exact antiresonance is supposed inside the arm cavities.
(iii) g_{xy}: a field enhancement factor for field y inside cavity x. The $x = {\rm a}, {\rm p}, {\rm s}$ denotes arm, power-recycling, and signal-extraction cavity, respectively. The field enhancement factor is a measure of how much the field is amplified inside the cavity, which usually gives a measure of the phase sensitivity to the signal, so it is a very important factor. For example, $g_{\rm p1} = t_{\rm p}/(1 - r_{\rm p} r_{\rm s} r_{\rm a1}^2)$ is for the PM sidebands inside the power-recycling cavity (and also inside the SEC, because they are exactly identical in this case); $g_{\rm p2} = t_{\rm p}/(1 + r_{\rm p} r_{\rm a2})$ is that for the AM sidebands

inside the power-recycling cavity.

(iv) δ_i: the demodulation phases, $i = 1, 2$ for PM (modulation 1) and AM (modulation 2).

(v) V_{xy}: the demodulated signal at signal port x ("b" for bright, "o" for pickoff, and "d" for dark port) with demodulation scheme y ("s" for single demodulation and "d" for double demodulation).

At the bright port, the sensitivities of the extracted signal $V_{\rm bd}$ for $l_{\rm p}$, l_-, and $l_{\rm s}$ are given as

$$\frac{\partial V_{\rm bd}}{\partial l_{\rm p}} \propto 8(g_{\rm p1}^2 r_{\rm a1}^2 r_{\rm s} r_{\rm p2} + r_{\rm p1} g_{\rm p2}^2 r_{\rm a2}) \cos\delta_1 \cos\delta_2$$

$$\frac{\partial V_{\rm bd}}{\partial l_{\rm s}} \propto 8 g_{\rm p1}^2 r_{\rm s} r_{\rm a1}^2 r_{\rm p2} \cos\delta_1 \cos\delta_2$$

$$\frac{\partial V_{\rm bd}}{\partial l_-} \propto 4 g_{\rm p1}^2 r_{\rm a1} r_{\rm p2} (1 - r_{\rm s}^2 r_{\rm a1}^2) \sin\delta_1 \cos\delta_2,$$

respectively. The signals at the pickoff port contain similar information as follows:

$$\frac{\partial V_{\rm od}}{\partial l_{\rm p}} \propto 8 \frac{r_{\rm p}}{t_{\rm p}} g_{\rm p1} g_{\rm p2} (g_{\rm p1} r_{\rm s} r_{\rm a1}^2 + g_{\rm p2} r_{\rm a2}) \cos\delta_1 \cos\delta_2$$

$$\frac{\partial V_{\rm od}}{\partial l_{\rm s}} \propto 8 \frac{r_{\rm p}}{t_{\rm p}} g_{\rm p1}^2 g_{\rm p2} r_{\rm s} r_{\rm a1}^2 \cos\delta_1 \cos\delta_2$$

$$\frac{\partial V_{\rm od}}{\partial l_-} \propto 4 \frac{r_{\rm p}}{t_{\rm p}} g_{\rm p1}^2 g_{\rm p2} r_{\rm a1} (1 + r_{\rm s}^2 r_{\rm a1}^2) \sin\delta_1 \cos\delta_2,$$

with slight differences that can be used to determine the polarity of the signal. In contrast, for the signals at the dark port, the signals are given as

$$\frac{\partial V_{\rm dd}}{\partial l_{\rm p}} = 0 \qquad \frac{\partial V_{\rm dd}}{\partial l_{\rm s}} = 0$$

$$\frac{\partial V_{\rm dd}}{\partial l_-} \propto 4 g_{\rm p1} t_{\rm s} r_{\rm a1} g_{\rm p2} g_{\rm s2} r_{\rm a2} \sin\delta_1 \cos\delta_2.$$

When the carrier and the modulation sidebands are on exact resonance or antiresonance inside the arm cavities, PRC and SEC, all parameters appearing in the above expressions become real quantities, so the signal sensitivities of demodulated signals depend only on the demodulation phases δ_i. For example, for $l_{\rm p}$ and $l_{\rm s}$, both error signals show the same dependences on the δ_i, which means that the two signals are completely "linearly dependent," in terms of demodulation phases, though the signal sensitivities are slightly different due to the finesse difference between PRC and SEC. Therefore, in this situation, it is quite difficult to extract two independent error signals for the PRC and SEC lengths.

B. "Delocation"

The idea to resolve this problem is to make use of an off-resonant condition of the light field(s). The simple way to realize this condition is to make the coupling cavity off-resonant for rf sidebands by a macroscopic detuning, as is shown in Fig. 3. The resonance condition of the carrier in the two cavities are maintained whereas the rf sidebands are slightly detuned inside the power-recycling cavity by changing the position of PRM [14]. This process, macroscopic detuning, will be named Delocation in the following.

Now the modified expressions for the error signals become somewhat more complex, as follows. For the signals at the bright port, the expressions are given as

$$\frac{\partial V_{\rm bd}}{\partial l_{\rm p}} \propto 8\,{\rm Re}[(g_{\rm p1}^2 r_{\rm s} r_{\rm a1}^2 r_{\rm p2u} + r_{\rm p1} g_{\rm p2u}^2 r_{\rm a2} e^{-i\Delta_2}) e^{-i\delta_2}] \cos\delta_1$$

$$\frac{\partial V_{\rm bd}}{\partial l_{\rm s}} \propto 8\,{\rm Re}[g_{\rm p1}^2 r_{\rm s} r_{\rm a1}^2 r_{\rm p2u} e^{-i\delta_2}] \cos\delta_1$$

$$\frac{\partial V_{\rm bd}}{\partial l_-} \propto -4\,{\rm Im}[g_{\rm p1}^2 r_{\rm a1} (e^{-i\Delta_1} - r_{\rm s}^2 r_{\rm a1}^2 e^{i\Delta_1}) e^{-i\delta_1}] \times {\rm Re}[r_{\rm p2u} e^{-i\delta_2}].$$

There are two effects: one is a slight off-resonance condition for AM appearing in $g_{\rm p2u}$, $r_{\rm p2u}$, and Δ_2, the other is the macroscopically extended PRC length for PM, typically appearing on Δ_1. Now $g_{\rm p2u} = t_{\rm p}/(1 + r_{\rm p} r_{\rm a2} e^{-i\Delta_2})$ and $r_{\rm p2u} = (r_{\rm p} - r_{\rm a2} e^{-i\Delta_2})/(1 + r_{\rm p} r_{\rm a2} e^{-i\Delta_2})$, field enhancement factor and reflectivity at the bright port for AM side-

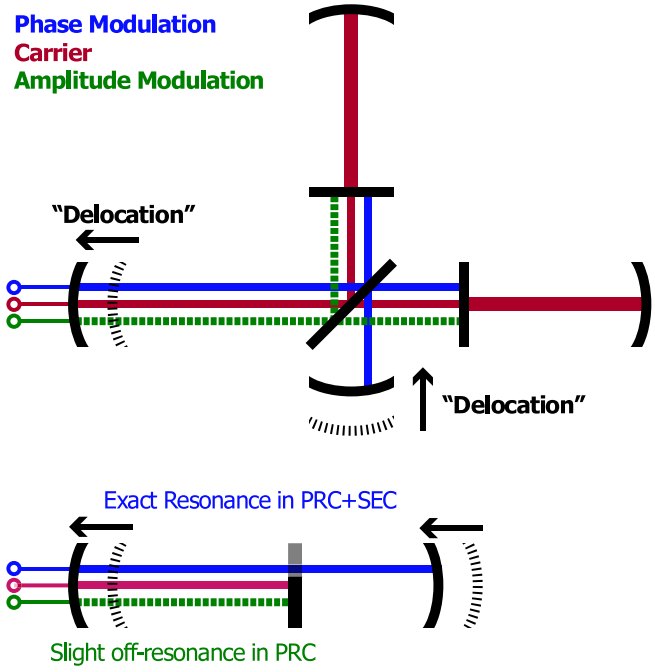

FIG. 3 (color online). The schematic of the idea "Delocation." The same color coding and legend as in Fig. 2 are used. The goal is to make (only) one of the modulations slightly off-resonant inside the cavity. By giving the same amount of macroscopic displacements to PRM and SEM, only AM sidebands will be detuned inside the power-recycling cavity, without affecting the PM sidebands and of course the carrier. The translation to the coupled cavity is also shown.

bands, respectively, have complex values instead of real values. The delocation effect is included in the delocation phase $\Delta_1 = l_{\rm del}\omega_1/c$ and $\Delta_2 = l_{\rm del}\omega_2/c$, where $l_{\rm del}$ is a macroscopic delocation. The signals at the pickoff port are again similar to those at the bright port as follows:

$$\frac{\partial V_{\rm od}}{\partial l_{\rm p}} \propto 8\frac{r_{\rm p}}{t_{\rm p}} g_{\rm p1}\,{\rm Re}[g_{\rm p2u}(g_{\rm p1}r_{\rm s}r_{\rm a1} + g_{\rm p2u}r_{\rm a2}e^{-i\Delta_2})e^{-i\delta_2}] \times \cos\delta_1$$

$$\frac{\partial V_{\rm od}}{\partial l_{\rm s}} \propto 8\frac{r_{\rm p}}{t_{\rm p}} g_{\rm p1}^2 r_{\rm s}r_{\rm a1}^2\,{\rm Re}[g_{\rm p2u}e^{-i\delta_2}]\cos\delta_1$$

$$\frac{\partial V_{\rm od}}{\partial l_{-}} \propto -4\frac{r_{\rm p}}{t_{\rm p}} g_{\rm p1}^2 r_{\rm a1}\,{\rm Im}[(e^{i\Delta_1} - r_{\rm s}^2 r_{\rm a1}^2 e^{-i\Delta_1})e^{-i\delta_1}] \times {\rm Re}[g_{\rm p2u}e^{-i\delta_2}].$$

As for the signals at the dark port,

$$\frac{\partial V_{\rm dd}}{\partial l_{\rm p}} = 0 \qquad \frac{\partial V_{\rm dd}}{\partial l_{\rm s}} = 0$$

$$\frac{\partial V_{\rm dd}}{\partial l_{-}} \propto 4 g_{\rm p1}t_{\rm s}r_{\rm a1}\,{\rm Re}[g_{\rm p2u}g_{\rm s2u}r_{\rm a2}e^{-i\delta_2}]\sin\delta_1.$$

This is because the relative phase between the carrier and modulation sidebands changes by applying the delocation. This also affects the demodulated signals as is shown above; however, the point is that the effect is different for all three signals. In other words, the optimum demodulation phase that maximizes these two signals can differ, depending on the degrees of delocation Δ_i. The $l_{\rm p}$ and $l_{\rm s}$ signals, for example, show exactly the same dependencies on δ_1, whereas different dependencies on δ_2 due to the complex quantities of $r_{\rm p2u}$, $g_{\rm p2u}$, and Δ_i. Therefore, by choosing an appropriate delocation phase, one can find an optimum demodulation phase where undesired signal disappear. Making use of these aspects, exact diagonalization of the sensing matrix is possible. The optimum delocation Δ_i is completely dependent on the optical parameters of the RSE interferometer.

Thus, the error signals for $l_{\rm p}$ and $l_{\rm s}$ can be separated by delocating the cavity properly, for the same reason with the coupled-cavity case [14]. In addition, the l_{-} signal appears nearly in the quadrature phase for δ_1, which is almost orthogonal to the other two signals extracted with exact in-phase demodulation. Therefore, l_{-} is also readily distinguishable from $l_{\rm p}$ and $l_{\rm s}$. In order to utilize this condition, it is important that modulation 1 is satisfying a particular resonance condition, otherwise the in-phase conditions for $l_{\rm p}$ and $l_{\rm s}$ do not hold. It is also important that modulation 2 does not reach the dark port, which means that there is in principle no signal at dark port for $l_{\rm p}$ and $l_{\rm s}$. This fact is also beneficial for clean signal extraction and robustness of the signal sensing matrix, which is another significant merit of this sensing scheme.

The numerical result of the sensing matrix is shown in Table III. A sensing matrix using the preliminary control scheme for LCGT is cited in Table II for comparison. In Table III, the signal sensitivities given by analytical expressions are listed together with the numerical results using the FINESSE simulation software. Analytical expressions for L-signals and l-signals with single demodulation are given in Appendix C. The off-diagonal values show quite a good agreement between the two methods. Slight differences in some of the off-diagonals are due to the different resonant conditions of two sets of sidebands for the arm cavities.

IV. CONCLUSION

A novel longitudinal sensing scheme for tuned RSE was newly proposed. In order to extract the error signals for the central part of the RSE interferometer, phase and amplitude modulations are suggested for the double-modulation scheme. Based on the concept of the PDH scheme, very simple allocations of the two sets of modulation sidebands are implemented, which enable an almost diagonal sensing matrix, a feature improved further by the delocation technique.

TABLE II. The length sensing matrix of preliminary control design for LCGT [15]. Five signals are extracted from each port, using the particular demodulation scheme with some demodulation phase(s) (shown in degree) to provide appropriate error signals. The matrix elements are normalized so that the diagonal elements become unity. The simulation software FINESSE was used to calculate the matrix elements. This design was also based on a double-modulation and demodulation scheme, but with different optical and modulation parameters. There were significant admixtures of the $\phi_{\rm p}$ degree of freedom to the extracted signals for ϕ_{-} and $\phi_{\rm s}$.

Port	Demodulation	δ_1	δ_2	$\partial/\partial\Phi_{+}$	$\partial/\partial\Phi_{-}$	$\partial/\partial\phi_{\rm p}$	$\partial/\partial\phi_{-}$	$\partial/\partial\phi_{\rm s}$
Bright	Single	95	$\cdots$	1	-4×10^{-6}	6×10^{-6}	-5×10^{-4}	-1×10^{-4}
Dark	Single	45	$\cdots$	0	1	0	1×10^{-3}	0
Dark	Double	135	270	8×10^{-3}	-3×10^{-4}	1	-3×10^{-2}	-6×10^{-2}
Pickoff	Double	67	180	1×10^{-2}	8×10^{-3}	1×10^{0}	1	6×10^{-2}
Bright	Double	277	180	4×10^{-3}	1×10^{-3}	1×10^{0}	1×10^{-1}	1

TABLE III. The numerical results of the length sensing matrix with the newly proposed sensing scheme. The numerical results using FINESSE software are also listed in **bold** form. Design values for LCGT were used for this calculation as optical parameters; $r_1 = r_3 = 0.996\,000$, $r_2 = r_4 = 0.999\,950$, $r_p = 0.80$, and $r_s = 0.77$. Throughout these calculations, the interferometer was assumed to be lossless for simplicity. The delocation l_{del} was chosen to give an optimized signal size [14], which corresponds to the delocation phase $\Delta_1 = 0.216°$ and $\Delta_2 = 1.296°$. The important contrast is that the signals for ϕ_p, ϕ_-, and ϕ_s are now almost completely separated.

Port	Demodulation	δ_1	δ_2	$\partial/\partial\Phi_+$	$\partial/\partial\Phi_-$	$\partial/\partial\phi_p$	$\partial/\partial\phi_-$	$\partial/\partial\phi_s$
Bright	Single	1.06	···	1	0	3.56×10^{-3}	0	2.56×10^{-3}
		3.56	···	**1**	$<$**10^{-14}**	**3.56 $\times$ 10^{-3}**	$<$**10^{-9}**	**2.56 $\times$ 10^{-3}**
Dark	Single	90.0	···	0	1	0	1.00×10^{-3}	0
		90.0	···	$<$**10^{-17}**	**1**	$<$**10^{-19}**	**1.00 $\times$ 10^{-3}**	$<$**10^{-19}**
Pickoff	Double	3.32	−69.2	1.00×10^{-3}	0	1	0	0
		3.56	**−69.2**	**1.00 $\times$ 10^{-3}**	$<$**10^{-11}**	**1**	$<$**10^{-13}**	$<$**10^{-14}**
Dark	Double	90.0	22.0	0	1.00×10^{-3}	0	1	0
		90.0	**21.8**	$<$**10^{-10}**	**1.00 $\times$ 10^{-3}**	$<$**10^{-6}**	**1**	$<$**10^{-13}**
Pickoff	Double	3.32	−28.0	1.00×10^{-3}	0	0	0	1
		3.56	**−28.0**	**1.15 $\times$ 10^{-3}**	$<$**10^{-9}**	$<$**10^{-13}**	$<$**10^{-8}**	**1**

ACKNOWLEDGMENTS

The authors are grateful to Albrecht Rüdiger for helpful discussions and comments. This research is supported in part by a Grant-in-Aid for Scientific Research on Priority Areas (415) of the Ministry of Education, Culture, Sports, Science and Technology, from Japan and also partially supported by National Science Foundation cooperative agreement No. PHY-0107417 from U.S. funding.

APPENDIX A: DOUBLE-MODULATION AND -DEMODULATION

In general, double modulation could be an arbitrary combination of phase and amplitude modulations; however, in this paper phase and amplitude modulations are assumed for double modulation.

Incoming laser light (carrier) is modulated using electro-optic modulators to produce modulation sidebands. To avoid the generation of subsidebands (sideband of sideband), parallel modulation instead of series modulation should be used. As a result, input fields will take the form

$$\begin{aligned} E_{in} &= E_0 e^{i\Omega_0 t} \rightarrow E_0(1 + \Gamma_2 \cos(\omega_2 t)) e^{i(\Omega_0 t + \Gamma_1 \cos(\omega_1 t))} \\ &\simeq E_0 e^{i\Omega_0 t}\left\{1 + i\Gamma_1(e^{i\omega_1 t} + e^{-i\omega_1 t}) \right. \\ &\quad \left. + \frac{\Gamma_2}{2}(e^{i\omega_2 t} + e^{-i\omega_2 t})\right\} \\ &\equiv E_0 e^{i\Omega_0 t} + E_1 e^{i(\Omega_0+\omega_1)t} + E_1 e^{i(\Omega_0-\omega_1)t} \\ &\quad + E_2 e^{i(\Omega_0+\omega_2)t} + E_2 e^{i(\Omega_0-\omega_2)t}, \end{aligned}$$

where the modulation depths Γ_i for the two modulations were assumed to be small enough so that the above approximation holds. Then these five frequencies of electric fields will have different responses from an optical system (RSE interferometer, in this case) depending on the optical frequencies. So the output fields will have the form of

$$\begin{aligned} E_{out} &= E_0 H_{x0} e^{i\Omega_0 t} + E_1 H_{x1u} e^{i(\Omega_0+\omega_1)t} + E_1 H_{x1l} e^{i(\Omega_0-\omega_1)t} \\ &\quad + E_2 H_{x2u} e^{i(\Omega_0+\omega_2)t} + E_2 H_{x2l} e^{i(\Omega_0-\omega_2)t}, \end{aligned}$$

where H_{xy} is a response of the field y (0 for carrier, 1u for upper and 1l for lower sideband of first modulation, 2u and 2l for those of second modulation) from incident point to the signal port x.

The reflection and pickoff ports are dedicated as signal-extraction ports, from which portions of the light fields are picked up, received with the photodetector, and then demodulated by a mixer with a local rf signal to produce error signals. The demodulated signals that are extracted from beat signals between the carrier and the phase modulation sidebands are given in general form as

$$\begin{aligned} V_{xd} &= 2\,\mathrm{Re}[((E_1 H_{x1l})^* E_2 H_{x2u} \\ &\quad + (E_2 H_{x2l})^* E_1 H_{x1u}) e^{-i\delta_1} e^{-i\delta_2} + ((E_1 H_{x1u})^* E_2 H_{x2u} \\ &\quad + (E_2 H_{x2l})^* E_1 H_{x1l}) e^{i\delta_1} e^{-i\delta_2}] \\ &= E_0^2 \Gamma_1 \Gamma_2\, \mathrm{Im}[(H_{x1u} H_{x2u} - H_{x2u} H_{x1u}) e^{-i\delta_1} e^{-i\delta_2} \\ &\quad + (H_{x1l} H_{x2u} - H_{x2u} H_{x1l}) e^{i\delta_1} e^{-i\delta_2}], \end{aligned}$$

where x denotes signal port, second subscript "d" means double demodulation ("s" for single demodulation), and δ_i is a demodulation phase; $\delta_i = 0$ corresponds to in-phase and $\delta_i = \pi/2$ to quadrature-phase demodulation.

The signal sensitivities to particular length changes are given by differentiating the above signal with corresponding degrees of freedom as

$$\begin{aligned} \frac{\partial V_{xd}}{\partial \phi_z} \propto \mathrm{Im}\Big[&\frac{\partial}{\partial \phi_z}(H_{x1u} H_{x2u} - H_{x2u} H_{x1u}) e^{-i\delta_1} e^{-i\delta_2} \\ &+ \frac{\partial}{\partial \phi_z}(H_{x1l} H_{x2u} - H_{x2u} H_{x1l}) e^{i\delta_1} e^{-i\delta_2} \Big] \end{aligned}$$

where z is the phase degree of freedom associated with the cavity lengths. The ideal demodulation process is assumed here, so all detection and demodulation efficiencies are set to be unity.

APPENDIX B: COMPLETE EXPRESSIONS OF THE RSE INTERFEROMETER

The optical-frequency-dependent transfer functions of the light fields from the input to all three signal ports are given in general form as

$$H_{\mathrm{by}}(\Phi_i,\phi_i)=\frac{-r_{\mathrm{p}}+\{\frac{1}{2}(r_{\mathrm{a2}}(\Phi_2)\mathrm{e}^{-\mathrm{i}\phi_2}+r_{\mathrm{a1}}(\Phi_1)\mathrm{e}^{-\mathrm{i}\phi_1})+\frac{(1/4)r_{\mathrm{s}}(r_{\mathrm{a2}}(\Phi_2)\mathrm{e}^{-\mathrm{i}\phi_2}-r_{\mathrm{a1}}(\Phi_1)\mathrm{e}^{-\mathrm{i}\phi_1})(r_{\mathrm{a2}}(\Phi_2)\mathrm{e}^{-\mathrm{i}\phi_4}-r_{\mathrm{a1}}(\Phi_1)\mathrm{e}^{-\mathrm{i}\phi_3})}{1-(1/2)r_{\mathrm{s}}(r_{\mathrm{a2}}(\Phi_2)\mathrm{e}^{-\mathrm{i}\phi_4}+r_{\mathrm{a1}}(\Phi_1)\mathrm{e}^{-\mathrm{i}\phi_3})}\}}{1-r_{\mathrm{p}}\{\frac{1}{2}(r_{\mathrm{a2}}(\Phi_2)\mathrm{e}^{-\mathrm{i}\phi_2}+r_{\mathrm{a1}}(\Phi_1)\mathrm{e}^{-\mathrm{i}\phi_1})+\frac{(1/4)r_{\mathrm{s}}(r_{\mathrm{a2}}(\Phi_2)\mathrm{e}^{-\mathrm{i}\phi_2}-r_{\mathrm{a1}}(\Phi_1)\mathrm{e}^{-\mathrm{i}\phi_1})(r_{\mathrm{a2}}(\Phi_2)\mathrm{e}^{-\mathrm{i}\phi_4}-r_{\mathrm{a1}}(\Phi_1)\mathrm{e}^{-\mathrm{i}\phi_3})}{1-(1/2)r_{\mathrm{s}}(r_{\mathrm{a2}}(\Phi_2)\mathrm{e}^{-\mathrm{i}\phi_4}+r_{\mathrm{a1}}(\Phi_1)\mathrm{e}^{-\mathrm{i}\phi_3})}\}}$$

$$H_{\mathrm{oy}}(\Phi_i,\phi_i)=\frac{t_{\mathrm{p}}}{1-r_{\mathrm{p}}\{\frac{1}{2}(r_{\mathrm{a2}}(\Phi_2)\mathrm{e}^{-\mathrm{i}\phi_2}+r_{\mathrm{a1}}(\Phi_1)\mathrm{e}^{-\mathrm{i}\phi_1})+\frac{(1/4)r_{\mathrm{s}}(r_{\mathrm{a2}}(\Phi_2)\mathrm{e}^{-\mathrm{i}\phi_2}-r_{\mathrm{a1}}(\Phi_1)\mathrm{e}^{-\mathrm{i}\phi_1})(r_{\mathrm{a2}}(\Phi_2)\mathrm{e}^{-\mathrm{i}\phi_4}-r_{\mathrm{a1}}(\Phi_1)\mathrm{e}^{-\mathrm{i}\phi_3})}{1-(1/2)r_{\mathrm{s}}(r_{\mathrm{a2}}(\Phi_2)\mathrm{e}^{-\mathrm{i}\phi_4}+r_{\mathrm{a1}}(\Phi_1)\mathrm{e}^{-\mathrm{i}\phi_3})}\}}$$

$$H_{\mathrm{dy}}(\Phi_i,\phi_i)=\frac{t_{\mathrm{p}}t_{\mathrm{s}}\frac{(1/2)(r_{\mathrm{a2}}(\Phi_2)\mathrm{e}^{-\mathrm{i}\phi_2/2}\mathrm{e}^{-\mathrm{i}\phi_4/2}-r_{\mathrm{a1}}(\Phi_1)\mathrm{e}^{-\mathrm{i}\phi_1/2}\mathrm{e}^{-\mathrm{i}\phi_3/2})}{1-(1/2)r_{\mathrm{s}}(r_{\mathrm{a2}}(\Phi_2)\mathrm{e}^{-\mathrm{i}\phi_4}+r_{\mathrm{a1}}(\Phi_1)\mathrm{e}^{-\mathrm{i}\phi_3})}}{1-r_{\mathrm{p}}\{\frac{1}{2}(r_{\mathrm{a2}}(\Phi_2)\mathrm{e}^{-\mathrm{i}\phi_2}+r_{\mathrm{a1}}(\Phi_1)\mathrm{e}^{-\mathrm{i}\phi_1})+\frac{(1/4)r_{\mathrm{s}}(r_{\mathrm{a2}}(\Phi_2)\mathrm{e}^{-\mathrm{i}\phi_2}-r_{\mathrm{a1}}(\Phi_1)\mathrm{e}^{-\mathrm{i}\phi_1})(r_{\mathrm{a2}}(\Phi_2)\mathrm{e}^{-\mathrm{i}\phi_4}-r_{\mathrm{a1}}(\Phi_1)\mathrm{e}^{-\mathrm{i}\phi_3})}{1-(1/2)r_{\mathrm{s}}(r_{\mathrm{a2}}(\Phi_2)\mathrm{e}^{-\mathrm{i}\phi_4}+r_{\mathrm{a1}}(\Phi_1)\mathrm{e}^{-\mathrm{i}\phi_3})}\}},$$

where $\phi_i=2l_i\Omega/c$ and $\Phi_i=2L_i\Omega/c$ are the round-trip phase of the arm and recycling cavities. The definitions for L_i, l_i are given in Fig. 1. The $r_{\mathrm{a}i}$ are the reflectivities of the arm cavities which are given as

$$r_{\mathrm{a1}}(\Phi_1)=\frac{-r_1+r_2\mathrm{e}^{-\mathrm{i}\Phi_1}}{1-r_1r_2\mathrm{e}^{-\mathrm{i}\Phi_1}}\qquad r_{\mathrm{a2}}(\Phi_2)=\frac{-r_3+r_4\mathrm{e}^{-\mathrm{i}\Phi_2}}{1-r_3r_4\mathrm{e}^{-\mathrm{i}\Phi_2}}.$$

APPENDIX C: *L*-SIGNALS AND *l*-SIGNALS WITH SINGLE DEMODULATION

Using these transfer functions and the demodulation procedure (Appendix A), analytic expressions for signal sensitivities are calculated. The bright and dark port signals for the L-signals using single demodulations are given as

$$\frac{\partial V_{\mathrm{bs}}}{\partial L_+}\propto 2r_2(g_{\mathrm{p0}}^2g_{\mathrm{a0}}^2r_{\mathrm{p1}}+2r_{\mathrm{p0}}g_{\mathrm{p1}}^2g_{\mathrm{a1}}^2r_{\mathrm{s}}r_{\mathrm{a1}})\cos\delta_1\qquad \frac{\partial V_{\mathrm{bs}}}{\partial L_-}\propto 2r_{\mathrm{p0}}g_{\mathrm{p1}}^2g_{\mathrm{a1}}^2r_2\mathrm{Im}[(\mathrm{e}^{\mathrm{i}\Delta_1}-r_{\mathrm{s}}^2r_{\mathrm{a1}}^2\mathrm{e}^{-\mathrm{i}\Delta_1})\mathrm{e}^{-\mathrm{i}\delta_1}]$$

$$\frac{\partial V_{\mathrm{bs}}}{\partial l_{\mathrm{p}}}\propto 4(-g_{\mathrm{p0}}^2r_{\mathrm{a0}}r_{\mathrm{p1}}+r_{\mathrm{p0}}g_{\mathrm{p1}}^2r_{\mathrm{s}}r_{\mathrm{a1}}^2)\cos\delta_1\qquad \frac{\partial V_{\mathrm{bs}}}{\partial l_{\mathrm{s}}}\propto 4(r_{\mathrm{p0}}g_{\mathrm{p1}}^2r_{\mathrm{s}}r_{\mathrm{a1}}^2)\cos\delta_1$$

$$\frac{\partial V_{\mathrm{bs}}}{\partial l_-}\propto 2r_{\mathrm{p0}}g_{\mathrm{p1}}^2r_{\mathrm{a1}}\,\mathrm{Im}[(\mathrm{e}^{\mathrm{i}\Delta_1}-r_{\mathrm{s}}^2r_{\mathrm{a1}}^2\mathrm{e}^{-\mathrm{i}\Delta_1})\mathrm{e}^{-\mathrm{i}\delta_1}]\qquad \frac{\partial V_{\mathrm{ds}}}{\partial L_+}=0\qquad \frac{\partial V_{\mathrm{ds}}}{\partial L_-}\propto -4g_{\mathrm{p0}}g_{\mathrm{s0}}g_{\mathrm{a0}}^2r_2g_{\mathrm{p1}}^2t_{\mathrm{s}}r_{\mathrm{a1}}\sin\delta_1$$

$$\frac{\partial V_{\mathrm{ds}}}{\partial l_{\mathrm{p}}}=0\qquad \frac{\partial V_{\mathrm{ds}}}{\partial l_{\mathrm{s}}}=0\qquad \frac{\partial V_{\mathrm{ds}}}{\partial l_-}\propto 2g_{\mathrm{p0}}g_{\mathrm{s0}}r_{\mathrm{a0}}g_{\mathrm{p1}}^2t_{\mathrm{s}}r_{\mathrm{a1}}\sin\delta_1.$$

The sensitivities of the double demodulated signals for L-signals are given as

$$\frac{\partial V_{\mathrm{bd}}}{\partial L_+}\propto 4r_2\,\mathrm{Re}[(2g_{\mathrm{p1}}^2g_{\mathrm{a1}}^2r_{\mathrm{a1}}r_{\mathrm{s}}r^{\mathrm{p2u}}+r_{\mathrm{p1}}g_{\mathrm{p2u}}^2g_{\mathrm{a2}}^2\mathrm{e}^{-\mathrm{i}\Delta_2})\mathrm{e}^{-\mathrm{i}\delta_2}]\cos\delta_1$$

$$\frac{\partial V_{\mathrm{bd}}}{\partial L_-}\propto -4\,\mathrm{Im}[g_{\mathrm{p1}}^2g_{\mathrm{a1}}^2r_2(\mathrm{e}^{-\mathrm{i}\Delta_1}-r_{\mathrm{s}}^2r_{\mathrm{a1}}^2\mathrm{e}^{\mathrm{i}\Delta_1})\mathrm{e}^{-\mathrm{i}\delta_1}]\,\mathrm{Re}[r_{\mathrm{p2u}}\mathrm{e}^{-\mathrm{i}\delta_2}]$$

$$\frac{\partial V_{\mathrm{od}}}{\partial L_+}\propto 4\frac{r_{\mathrm{p}}}{t_{\mathrm{p}}}g_{\mathrm{p1}}r_2\,\mathrm{Re}[g_{\mathrm{p2u}}(2g_{\mathrm{p1}}g_{\mathrm{a1}}^2r_{\mathrm{a1}}r_{\mathrm{s}}+g_{\mathrm{p2u}}g_{\mathrm{a2}}^2\mathrm{e}^{-\mathrm{i}\Delta_2})\mathrm{e}^{-\mathrm{i}\delta_2}]\cos\delta_1$$

$$\frac{\partial V_{\mathrm{od}}}{\partial L_-}\propto -4\frac{r_{\mathrm{p}}}{t_{\mathrm{p}}}g_{\mathrm{p1}}^2g_{\mathrm{a1}}^2r_2\,\mathrm{Im}[(\mathrm{e}^{-\mathrm{i}\Delta_1}-r_{\mathrm{s}}^2r_{\mathrm{a1}}^2\mathrm{e}^{\mathrm{i}\Delta_1})\mathrm{e}^{-\mathrm{i}\delta_1}]\,\mathrm{Re}[g_{\mathrm{p2u}}\mathrm{e}^{-\mathrm{i}\delta_2}]\qquad \frac{\partial V_{\mathrm{dd}}}{\partial L_+}=0$$

$$\frac{\partial V_{\mathrm{dd}}}{\partial L_-}\propto -8g_{\mathrm{p1}}t_{\mathrm{s}}r_{\mathrm{a1}}g_{\mathrm{a2}}^2r_2\,\mathrm{Re}[g_{\mathrm{p2u}}g_{\mathrm{s2u}}\mathrm{e}^{-\mathrm{i}\delta_2}]\sin\delta_1.$$

[1] B. Barish and R. Weiss, Phys. Today **52**, No. 10, 44 (1999); A. Abramovici, W. E. Althouse, R. W. P. Drever, Y. Gürsel, S. Kawamura, F. J. Raab, D. Shoemaker, L. Sievers, R. E. Spero, K. S. Thome, R. E. Vogt, R. Weiss, S. E. Whitcomb, and M. E. Zucker, Science **256**, 325 (1992); C. Bradaschia *et al.*, Nucl. Instrum. Methods Phys. Res., Sect. A **289**, 518 (1990); F. Acernese *et al.*, Classical Quantum Gravity **19**, 1421 (2002); K. Danzmann, in *First E. Amaldi Conference on Gravitational Wave Experiments*, edited by E. Coccia, G. Pizzella, and F. Ronga (World Scientific, Singapore, 1994), pp. 100–111; B. Willke *et al.*, Classical Quantum Gravity **19**, 1377 (2002); K. Tsubono, in First E. Amaldi Conference on Gravitational Wave Experiments, pp. 112–114; M. Ando *et al.*, Classical Quantum Gravity **19**, 1409 (2002).

[2] P. Fritschel, Proc. SPIE-Int. Soc. Opt. Eng. **4856**, 282 (2003).

[3] K. Kuroda *et al.*, Int. J. Mod. Phys. D **8**, 557 (1999).

[4] J. Mizuno, K. A. Strain, P. G. Nelson, J. M. Chen, R. Schilling, A. Rüdiger, W. Winkler, and K. Danzmann, Phys. Lett. A **175**, 273 (1993).

[5] M. Regehr, Ph.D. thesis, California Institute of Technology, Pasadena, California, 1995.

[6] A. Freise, http://www.rzg.mpg.de/~adf/, 2005.

[7] R. W. P. Drever, J. L. Hall, F. V. Kowalski, J. Hough, G. M. Ford, A. J. Munley, and H. Ward, Appl. Phys. B **31**, 97 (1983).

[8] M. W. Regehr, F. J. Raab, and S. E. Whitcomb, Opt. Lett. **20**, 1507 (1995).

[9] J. E. Mason and P. A. Willems, Appl. Opt. **42**, 1269 (2003).

[10] G. Müller, T. Delker, D. B. Tanner, and D. Reitze, Appl. Opt. **42**, 1283 (2003).

[11] D. A. Shaddock, M. B. Gray, C. Mow-Lowry, and D. E. McClelland, Appl. Opt. **42**, 1296 (2003).

[12] O. Miyakawa *et al.*, Phys. Rev. D **74**, 022001 (2006).

[13] F. Kawazoe, K. Kokeyama, S. Sato, O. Miyakawa, K. Somiya, M. Fukushima, N. Arai, S. Kawamura, and A. Sugamoto, J. Phys.: Conf. Ser. **32**, 380 (2006).

[14] S. Sato, K. Kokeyama, F. Kawazoe, K. Somiya, and S. Kawamura, J. Phys.: Conf. Ser. **32**, 470 (2006).

[15] S. Kawamura, http://tamago.mtk.nao.ac.jp/rse/LCGTdesign/RSE_design.pdf, 2002 (in Japanese).